

## Supporting information

# Low density magnetic silicate-nickel alloy composite hollow structures: seeds induced direct assembly fabrication and catalytic property

Gaiping Du<sup>1,2</sup>, Bin Liao<sup>1</sup>, Ran Liu<sup>1,2</sup>, Zhenguo An<sup>\*1</sup>, Jingjie Zhang<sup>\*1</sup>

(1. Key Laboratory of Photochemical Conversion and Optoelectronic Materials,  
Technical Institute of Physics and Chemistry, Chinese Academy of Sciences, Beijing  
100190, P. R. China; 2. University of Chinese Academy of Sciences, Beijing 100049,  
P. R. China)

\*To whom correspondence should be addressed. *Technical Institute of Physics and Chemistry, Chinese Academy of Sciences, Beijing 100190 China. Tel/fax: +86 10 82543690.*

E-mail: [zgan@mail.ipc.ac.cn](mailto:zgan@mail.ipc.ac.cn) (ZG An); [jjzhang@mail.ipc.ac.cn](mailto:jjzhang@mail.ipc.ac.cn) (JJ Zhang).

**Table S1.** Summary of the physical parameters of HGMs.

Sample	$d_m$ ( $\mu\text{m}$ )	$\rho_t$ ( $\text{g}/\text{cm}^3$ )
HGMs	50	0.38

Where  $d_m$  presents the mean particle size,  $\rho_t$  presents true density.

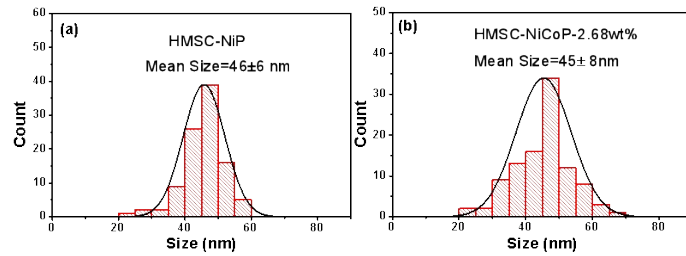


**Fig.S1** The size distribution of NPs in (a) HMSC-NiP, (b) HMSC-NiCoP-2.68wt%.

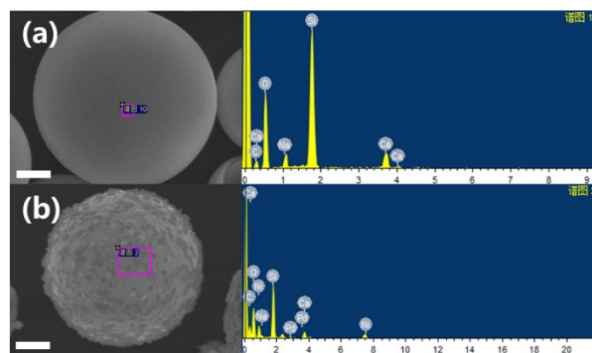


**Fig.S2** The SEM images of the (a) HGMs, (b) HMSC-Ni. The EDX results of (c) HGMs (d) HMSC-Ni. Scale bars, 10  $\mu\text{m}$ .

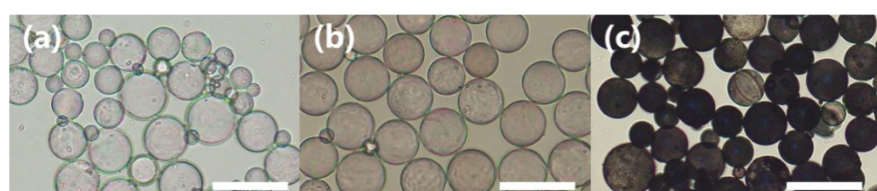


**Fig.S3** The Optical Microscopy images of (a) HGMs, (b) AHGMs, (c) HMSC-NiCoP-

2.68wt%. Scale bars, 100 $\mu$ m.

**Table S2.** Loading amounts measured by XRF and the rate constant of different loading amounts of HMSC-NiCoP. Where  $k_A$  refers to apparent rate constant,  $k_N$  presents mass normalized rate constant.

Samples	Loading (wt%)	$k_A$ (10 <sup>-3</sup> s <sup>-1</sup> )	$k_N$ (s <sup>-1</sup> g <sup>-1</sup> )
HMSC-NiCoP-0.314%	0.314	4.08	12.9
HMSC-NiCoP-0.586%	0.586	4.08	6.96
HMSC-NiCoP-1.34%	1.34	7.00	5.22
HMSC-NiCoP-2.14%	2.14	33.5	15.6
HMSC-NiCoP-2.68%	2.68	37.4	14.0
HMSC-NiCoP-2.93%	2.93	27.7	9.45
HMSC-NiCoP-3.14%	3.14	16.6	5.29
HMSC-NiCoP-3.48%	3.48	14.8	4.25
HMSC-NiCoP-6.00%	6.00	9.08	1.51

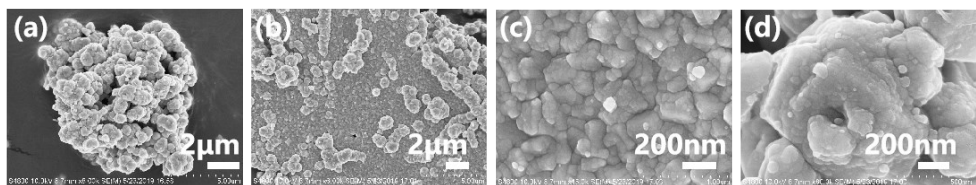


**Fig.S4** SEM images of pure NiCoP without HGMs.

As is shown in Fig.S4, the coalescence of NiCoP without HGMs support is obviously serious. It is further illustrated that HGMs support is necessary for active NPs to improve its stability.

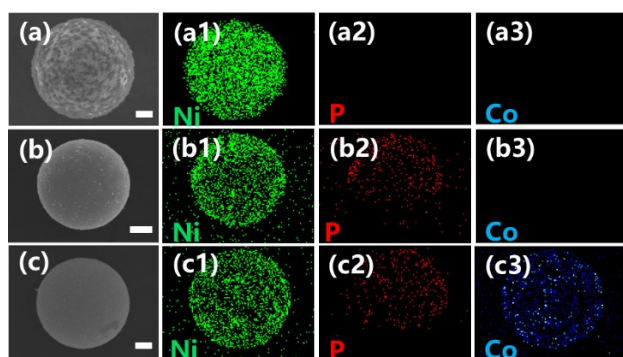


**Fig.S5** The energy dispersive spectrometer X-ray (EDX) element mapping patterns of (a) HMSC-Ni, (b) HMSC-NiP, (c) HMSC-NiCoP-2.68wt%; Scale bars, 10 μm.

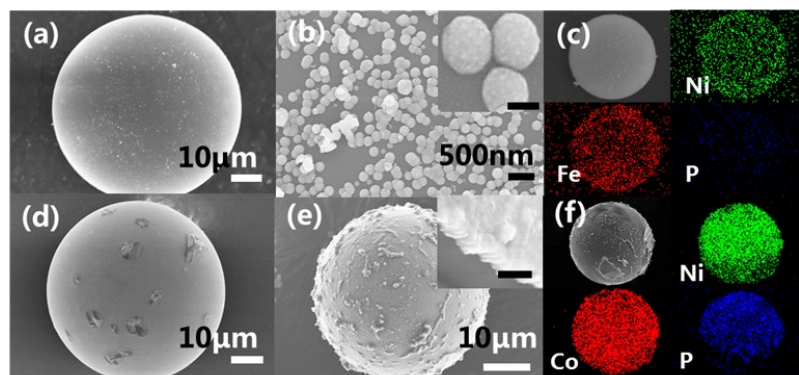


**Fig.S6** SEM images of depositing other metallic alloy on different supported spheres, (a) HGMs, (b) HMSC-NiFeP, inset of panel is the enlargement of superficial alloy particles. Scale bars, 100nm. (c) the elemental mapping of HMSC-NiFeP, (d) hollow phenolic resin

microspheres (HPRMs), (e) HPRM-NiCoP, inset of panel is the enlargement of the shell cross section. Scale bars, 500nm. (f) the elemental mapping of HPRM-NiCoP.

The seeds induced direct assembly approaches reported here holds the potential to be extended to the directed formation of other metallic NPs on various supports. As shown in Fig.S6, we have successfully realized the directed assembly of NiFeP NPs on AHGMs, and the nickel-based NPs on hollow phenolic resin microspheres. The elemental mapping by EDX illustrates the successful fabrication of diverse alloy materials on different supports. It is further certified that our seeds induced direct assembly fabrication is highly universal.

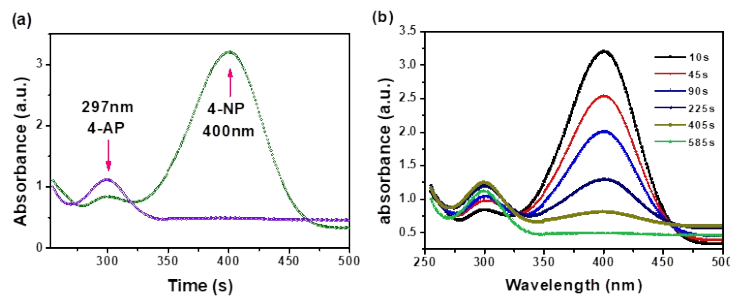


**Fig.S7** Typical time-dependent UV-Vis spectra, showing (a) the change in absorbance before and after the catalytic reaction of *p*-nitrophenol (4-NP) to *p*-aminophenol (4-AP) and (b) the absorbance evolutions by NaBH<sub>4</sub> using HMSC-NiCoP-2.68wt%.

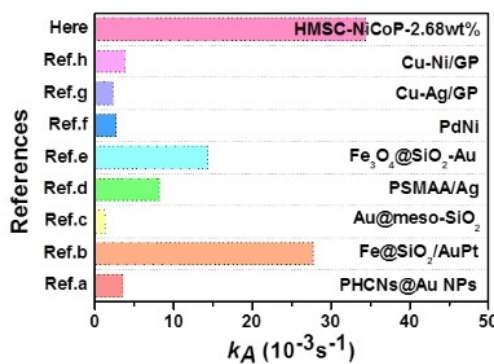


**Fig.S8** The  $k_A$  of HMSC-NiCoP-2.68wt% and the reported supported noble metal catalysts

and alloy catalysts used in catalyzing the 4-NP conversion. (Ref.a<sup>7</sup>, Ref.b<sup>30</sup>, Ref.c<sup>31</sup>, Ref. d<sup>32</sup>, Ref.e<sup>2</sup>, Ref.f<sup>33</sup>, Ref.g<sup>34</sup>, Ref.h<sup>34</sup>)

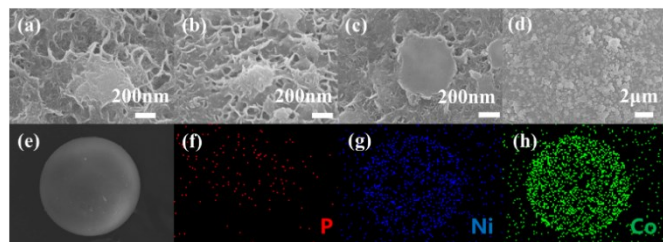


**Fig.S9** The SEM and EDX elemental mapping images of the synthesized catalytic materials after cyclic catalysis.

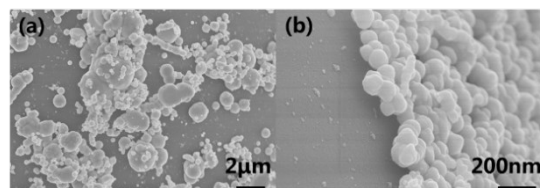


**Fig.S10** SEM images of (a) re-deposit the alloy species on HMSC-NiCoP-2.68wt% used after 7 cycles, (b) re-deposit the alloy species on HMSC-NiCoP-2.68wt% used after 1 cycle.

**Table S3.** XPS peak parameters of HMSC-Ni.

---

Peaks (Ni 2p)	Position(eV)	Area	FWHM(eV)

---

---

$\lambda_I$	880.49	3300.00	6.80
$\mu_I$	873.83	2457.00	3.43
$\nu_I$	869.50	213.59	1.40
$\lambda_2$	862.15	3068.80	4.36
$\mu_2$	856.20	4992.82	3.25
$\nu_2$	852.49	547.07	1.92

---

**Table S4.** XPS peak parameters of HMSC-NiP

---

Peaks (Ni 2p)	Position(eV)	Area	FWHM(eV)
$\lambda_I'$	880.25	1056.00	5.30
$\mu_I'$	874.13	1258.88	4.49
$\nu_I'$	870.03	252.37	2.47
$\lambda_2'$	861.69	1137.40	4.53
$\mu_2'$	856.16	1721.60	3.10
$\nu_2'$	852.89	740.26	1.82

---

Peaks (P 2p)	Position(eV)	Area	FWHM(eV)
$\gamma_I'$	132.90	108.54	3.29
$\phi_I'$	129.56	98.90	2.12

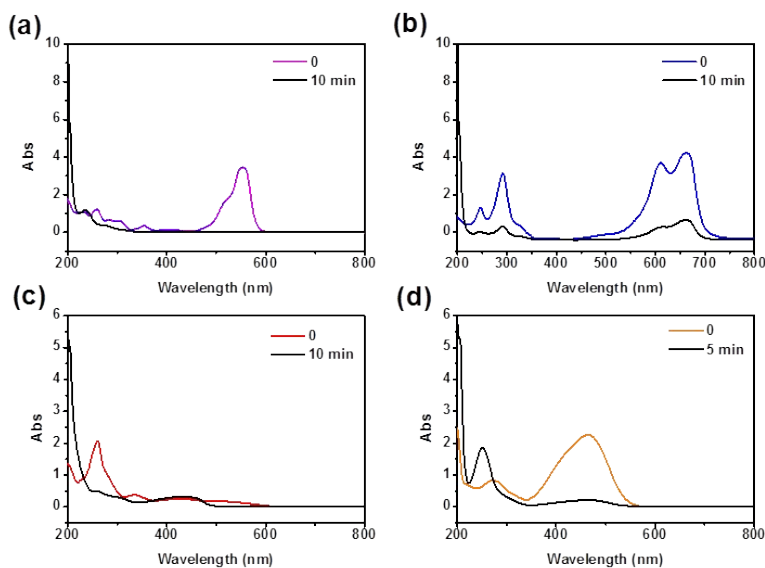
**Table S5.** XPS peak parameters of HMSC-NiCoP-2.68wt%.

Peaks (Ni 2p)	Position(eV)	Area	FWHM(eV)
$\lambda_I''$	881.11	3500.00	1.48
$\mu_I''$	874.45	2500.00	3.13
$\nu_I''$	870.86	1274.22	3.10
$\lambda_2''$	862.28	1908.00	2.66
$\mu_2''$	856.83	3700.00	2.84
$\nu_2''$	853.39	1349.26	6.50

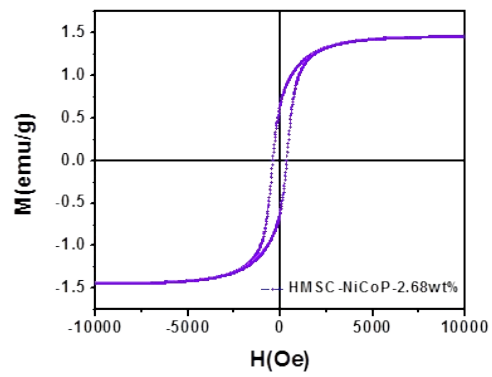
  

Peaks (Co 2p)	Position(eV)	Area	FWHM(eV)
$\delta_I''$	803.48	127.86	2.73

Peaks (P 2p)	Position(eV)	Area	FWHM(eV)
$\eta_1''$	798.10	300.00	3.52
$\delta_2''$	786.49	163.91	3.31
$\eta_2''$	781.47	600.00	3.77
<hr/>			
Peaks (P 2p)	Position(eV)	Area	FWHM(eV)
$\gamma_1''$	132.76	81.16	1.88
$\phi_1''$	129.61	114.64	1.60
<hr/>			



**Fig.S11** Corresponding absorbance curves at different wavelength of (a) RhB, (b) MB, (c) ArS, (d) MO before and after by NaBH<sub>4</sub> using synthesized HMSC-NiCoP-2.68wt%



**Fig.S12** Hysteresis loop of HMSC-NiCoP-2.68wt%.